Mon. Not. R. astr. Soc. (1982) **201**, 1095–1117

A study of the Chamaeleon dark cloud complex: survey, structure and embedded sources

A. R. Hyland and T. J. Jones *Mount Stromlo and Siding Spring Observatories, Research School of Physical Sciences, Australian National University, Canberra, Australia*

R. M. Mitchell *School of Physics, RAAF Academy, University of Melbourne, Melbourne, Australia*

Received 1982 May 15; in original form 1982 February 2

Summary. A 2 μm-survey of a significant fraction of the Chamaeleon dark cloud complex is presented. IR (*JHK*) photometry and CVF spectrophotometry of the sources found provide the following significant results.

(1) Discrimination between background field stars and cloud members shows an increase in the number of pre-main-sequence (PMS) members (over that found optically) by more than 50 per cent, corresponding to a star formation efficiency of ~12 per cent over the whole cloud. Similarly large numbers of hidden PMS objects are probably also present (and yet to be discovered) in other dark cloud regions.

(2) The number density of PMS objects within the Cloud ($> 8\,\mathrm{pc}^{-3}$) is close to that required by Norman & Silk to account for molecular velocity fields within dark clouds.

(3) The density structure of the Cloud, derived from the reddening of background field stars shows that small-scale clustering of two groups of PMS members seems to occur preferentially near steep density gradients in the cloud.

(4) The derived intrinsic infrared colours of the PMS objects are successfully reproduced by dust shell models presented in Section 5 for entirely reasonable ($\tau_{1\,\mu\mathrm{m}} \sim 1$) values of the optical depth.

(5) The models suggest that the observation of significant far IR radiation from some T Tauri objects results from some non-continuous form of the shell density distribution.

1 Introduction

Dark cloud complexes such as those in Taurus, Chamaeleon and R CrA are key regions for understanding the physical processes of low mass ($1-2\,M_\odot$) star formation. Emission-line T Tauri stars and embedded infrared sources (generally accepted as being pre-main-sequence

'PMS' objects) are universally associated with such complexes. Of particular interest are the structure of the complexes, the number of PMS members and the efficiency of star formation, the possible triggering mechanisms for low mass star formation, and the nature of the PMS objects themselves.

Historically, optical studies of the stellar content of dark cloud complexes e.g., Cohen & Kuhi (1979), have been hampered by obscuration within the clouds, and the objects considered are thus biased towards the front surface of the clouds. To overcome this problem, infrared surveys have become increasingly important since the pioneering work of Grasdalen, Strom & Strom (1973) and Vrba *et al.* (1975), but even these are subject to major limitations. The contribution of such studies to the understanding of dark clouds and PMS objects has been reviewed by Hyland (1980), who emphasizes the importance of discriminating members (a limitation first recognized by Elias 1978a, b, c).

The Chamaeleon dark cloud complex is a nearby region comprising an elongated dust cloud, a significant number of emission-line T Tauri stars, and three conspicuous reflection nebulae (Henize 1963; Hoffmeister 1962). This region has been the subject of a number of photometric and spectroscopic studies. Henize & Mendoza (1973), hereafter HM, discussed the spectra of some 32 emission-line stars within the complex: Schwartz (1977) discovered several Herbig–Haro objects within the region, and Appenzeller (1977, 1979) reported the presence of a high percentage of YY Ori-type spectra among the emission-line stars.

Glass (1979) obtained *JHKL* photometry of the majority of HM emission-line stars, and of an optical selection of apparent background objects. These latter appeared to follow a normal interstellar reddening curve in the near infrared (similar to that given by Jones & Hyland 1980) while the emission-line objects occupied a displaced locus in the $(J-H)$ versus $(H-K)$ diagram similar to that of the T Tauri stars in Taurus (see e.g., Hyland 1980, fig. 8). However, the reddening law in Chamaeleon at optical wavelengths remains in doubt. From photometry and spectroscopy of objects within the Chamaeleon region, both Grasdalen *et al.* (1975) and Rydgren (1980) derive anomalous values of $R = A_V/E(B-V)$ within the cloud ($R = 5.5$ and 5.0 respectively). These analyses cast doubt on the presently derived distance to the complex.

Despite these problems the Chamaeleon region is ideal for a detailed study of low mass PMS objects and their interaction with their placental dark cloud: it is close ($\leqslant 200$ pc), substantially out of the galactic plane ($b \sim -15°$) and contains a significant population of young objects.

In this paper we present a study of a considerable fraction of the Chamaeleon dark cloud complex and its embedded PMS objects, free from the limitations of previous work. We have undertaken an infrared survey at 2.2 μm to 10.5–11 mag, which is deep enough to reveal the majority of embedded PMS objects. We have made a careful attempt to identify the association and background objects and used the latter to derive the density structure of the cloud. The number of association members has been used to derive an estimate of the efficiency of star formation within the region, while their spatial distribution has allowed an examination of clustering within the cloud. Finally, the near-infrared properties of the identified PMS objects are analysed in terms of model dust shell structures.

2 Observations

2.1 THE 2 μm SURVEY

A 2.2 μm survey of 1400 square arcmin of the Chamaeleon T Association has been made using the AAO infrared photometer/spectrometer attached to the $f/15$ focus of the 3.9-m Anglo-Australian telescope. The detector was a solid nitrogen cooled InSb photovoltaic

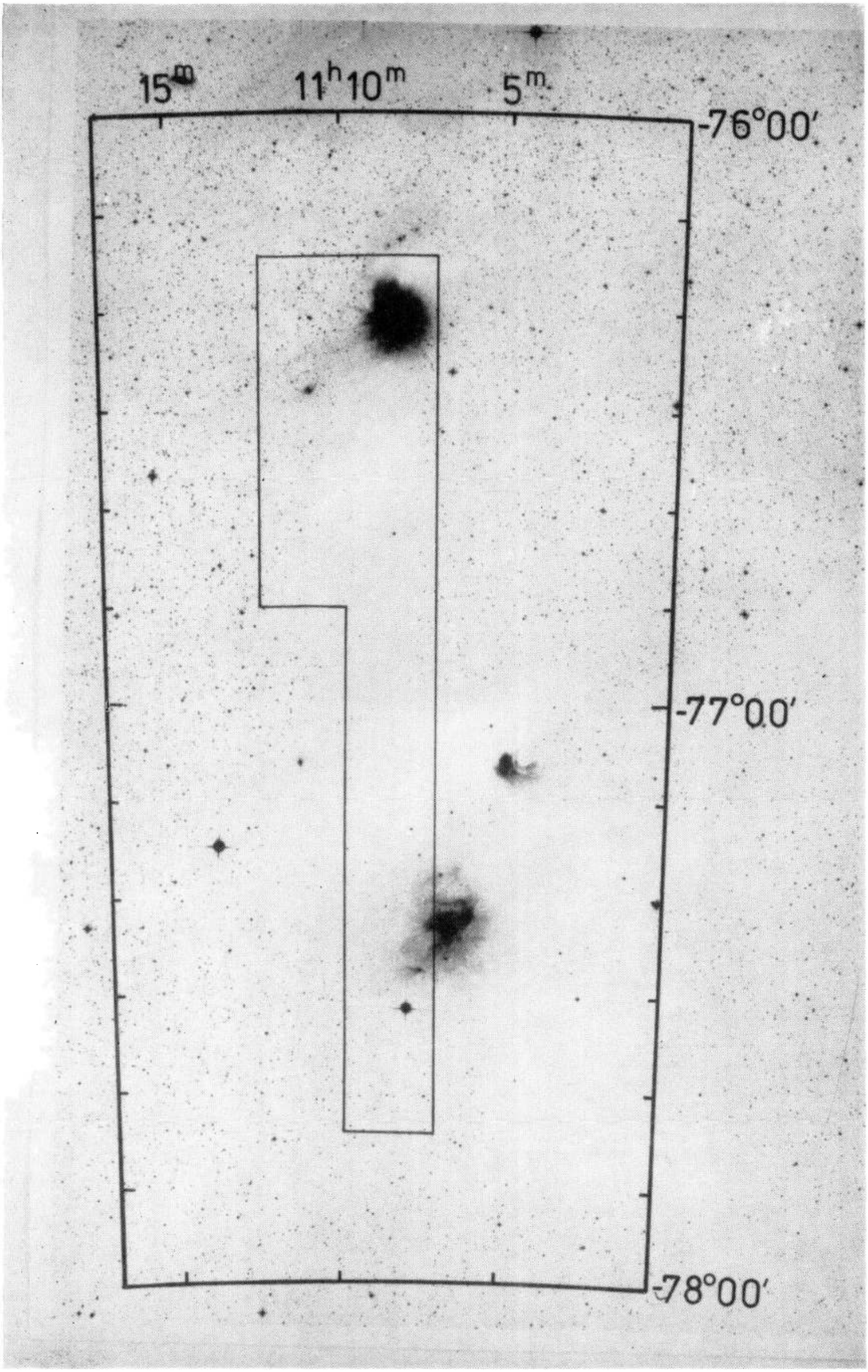

Plate 1. A photograph of the Chamaeleon dark cloud region indicating the boundaries of the infrared survey.

[*facing page* 1096]

Table 1. Scan centres for 9 × 9 arcmin blocks.

Block	RA	(1950) Dec
C1	11 08 25.0	– 76 19 00
C2	11 08 25.0	– 76 28 00
C3	11 08 25.0	– 76 37 00
C4	11 08 25.0	– 76 46 00
C5	11 08 25.0	– 76 55 00
C6	11 08 25.0	– 77 04 00
C7	11 08 25.0	– 77 13 00
C8	11 08 25.0	– 77 22 00
C9	11 08 25.0	– 77 31 00
C10	11 08 25.0	– 77 40 00
E1	11 10 57.0	– 76 19 00
E2	11 10 57.0	– 76 28 00
E3	11 10 57.0	– 76 37 00
E4	11 10 57.0	– 76 46 00

detector. The scans were made in blocks of 9 × 9 arcmin each, running in two north–south strips, one corresponding to the region of peak visual absorption, and the other 9 arcmin to the east. We call these the central and eastern blocks respectively. Positions of the block centres are given in Table 1, and the total area covered by the survey is marked on Plate 1. For the central strip, the survey was complete to $K = 10.5$, while for the eastern blocks (observed during cooler weather), the limiting magnitude was $K = 11.5$. The majority of observations were made during 1979 January to April.

The telescope was used in the automatic raster scan mode (Straede & Wallace 1976), and scanning of each block was performed at a rate of 40 arcsec s^{-1}, through a 3-mm aperture (~ 10.7 arcsec) and with a line spacing of 10 arcsec. This required approximately 12 min per block. Positions of the sources found in the survey were obtained from the scan data, and where possible were subsequently improved during the photometric observations. These are given in Table 2, together with the photometry below.

2.2 PHOTOMETRY

JHK photometry of 65 of the 109 sources found in the above survey was obtained with the same AAO IRPS during 1979, while an additional 13 were measured with the Mt Stromlo infrared photometer attached to the Mt Stromlo 1.9-m telescope. The measurements are listed in Table 2, and are on the AAT photometric system, which has been shown to be similar to the original Johnson system (Jones & Hyland 1980). The Mt Stromlo observations were all made during 1980 April. Several of the objects measured are emission-line objects and background stars for which IR photometry has previously been reported (Glass 1979). Comparison of observations of five apparently non-variable objects with the present photometry shows that the following transformations should probably be applied between the two photometric systems: $(J-H)_{AAO} = (J-H)_G\, 1.07 + 0.02$, $(H-K)_{AAO} = (H-K)_G + 0.02$, $K_{AAO} = K_G + 0.02$. These transformations have been applied to all subsequent comparisons of data on the two systems. Lower quality infrared data published earlier (Grasdalen *et al.* 1975) agrees within the quoted errors.

2.3 INFRARED SPECTROSCOPY

CVF spectra in the region 2.1–2.4 μm, and with a resolution of 2 per cent, were obtained for four of the redder objects in the survey, using the AAO IRPS. These spectra are displayed in Fig. 1 and discussed in Section 3.1.

Table 2. Infrared photometry.

SOURCE	RA (1950)	DEC	K	J-H	H-K	DATE	(7)[a]	(8)[b]	NOTES	E(J-K)
C1-1	11 09 14.9	-76 15 26	9.16	.98	.27	4/79	B	-	e	.57
C1-2	11 08 20.7	-76 16 24	9.25	2.51	1.48	4/79	M	-	c,e	
C1-3	11 07 52.0	-76 17 20	10.24	2.14	1.00	4/79	?	-	e	2.31?
C1-4	11 08 29.7	-76 17 15	9.91	1.52	.59	4/79	B	-	e	1.38
C1-5	11 08 19.4	-76 18 13	8.42	2.16	1.67	4/79	M	H 23	c,d,e	
C1-6	11 07 49.5	-76 18 19	9.22	2.50	1.54	4/79	M	-	c,e	
C1-7	11 08 26.1	-76 18 44	6.06	1.57	1.17	4/79	M	H 24	c,d,e	
C1-8	11 08 37.5	-76 19 13	8.84	1.51	.64	4/79	B	-	e	1.37
C1-9	11 08 30.8	-76 19 29	9.29	1.04	.39	4/79	B	-	d,e	.66
C1-10	11 07 08.5	-76 19 54	9.33	1.02	.35	4/79	B	-	e	.63
C1-11	11 08 16.6	-76 20 33	7.20	.33	.18	4/79	M	HD 97300	e	.50
C1-12	11 08 56.0	-76 21 03	9.12	1.34	.44	4/79	B	-	e	1.11
C1-13	11 07 40.7	-76 21 39	9.71	.97	.30	4/79	B	-	e	.56
C2-1	11 09 01.8	-76 24 25	10.21	1.74	.68	4/79	B	-	e	1.71
C2-2	11 07 52.1	-76 25 52	9.64	1.35	.46	4/79	B	-	e	1.13
C2-3	11 08 12.7	-76 27 38	10.20	1.19	.61	4/79	M	-	e	
C2-4	11 08 18.2	-76 29 30	9.36	1.52	.58	4/79	B	-	e	1.38
C2-5	11 09 21.5	-76 29 16	9.97	.92	.50	4/79	M	-	e	
C3-1	11 07 23.0	-76 35 13	10.29	.99	.27	4/79	B	-	e	.59
C3-2	11 09 37.0	-76 41 05	8.68	1.28	.44	4/79	B	= E3-5	e	1.02
C4-1	11 08 20.1	-76 41 44	10.11	1.36	.53	4/79	B	-	e	1.14
C4-2/3	11 08 20.1	-76 42 42	8.76	.60	.21	4/79	B	-	d,e	.60
C4-4	11 07 32.8	-76 44 36	8.50	1.19	.39	4/79	B	-	e	.89
C4-5	11 07 24.8	-76 45 58	9.85	1.24	.78	4/79	M	H 21	e	
C4-6	11 07 25.5	-76 48 36	7.50	1.34	.45	4/79	B	-	e	1.11
C4-7	11 09 31.5	-76 50 10	10.16	1.17	.39	4/79	B	-	e	.86
C5-1	11 07 35.0	-76 51 30	9.40	1.09	.35	2/80	B	-	e	
C5-2	11 09 21.5	-76 53 11	8.89	1.10	.39	2/80	B	-	e	
C5-3	11 08 09.0	-76 54 24	9.16	1.81	.74	2/80	B	-	e	
C5-4	11 07 52.6	-76 57 42	8.65	1.34	.50	2/80	B	-	e	
C6-1	11 07 12.0	-76 59 47	9.09	1.25	.70	2/80	M	H 20	d,e	
C6-2	11 08 59.7	-77 00 43	10.79	.69	.31	2/80	B?	-	e	
C6-4	11 09 36.7	-77 01 42	10.12	1.01	.34	2/80	B	-	e	
C6-5	11 08 28.3	-77 02 08	9.91	1.92	.82	2/80	B	-	e	
C6-6	11 07 21.5	-77 02 08	10.72	1.90	.81	2/80	B	-	e	
C7-1	11 08 15.5	-77 09 43	10.61	1.24	.58	2/80	M	-	e	
C7-2	11 07 59.4	-77 10 08	9.30	1.57	.61	2/80	B	-	e	
C7-3	11 08 31.7	-77 10 17	9.96	1.58	.61	2/80	B	-	e	
C7-5	11 08 10.3	-77 10 19	10.66	1.54	.60	2/80	B	-	e	
C7-7	11 07 43.4	-77 13 08	8.63	.80	.22	4/80	B	-	f	
C7-8	11 09 38.9	-77 15 10	6.32	1.31	.52	4/80	B	-	f	
C7-10	11 07 28.3	-77 15 50	8.34	1.03	.30	4/80	B	-	f	
C7-11	11 09 08.2	-77 16 34	8.29	1.05	.49	4/80	M	-	f	
C8-3	11 08 29.9	-77 20 59	8.55	1.08	.59	4/80	M	H 25	f	
C9-1	11 07 25.6	-77 27 23	10.66	1.86	1.32	4/80	M	-	f	
C9-2	11 07 12.2	-77 27 37	7.83	1.96	1.20	4/80	M	-	f	
C9-3	11 07 19.9	-77 27 43	7.87	2.07	1.19	4/80	M	-	f	
C9-4	11 08 23.1	-77 29 30	8.60	1.26	.40	4/80	B	-	f	
C9-5	11 07 50.4	-77 31 28	7.47	.24	.04	4/80	?	HD 97240	f	
C10-6	11 08 47.5	-77 41 48	8.73	1.04	.29	4/80	B	-	f	
C10-8	11 07 38.9	-77 44 13	8.99	.91	.26	4/80	B	-	f	
C10-9	11 09 26.2	-77 44 37	7.71	1.18	.35	4/80	B	-	f	
E1-1	11 09 44.7	-76 16 13	9.61	.94	.22	4/79	B	-	e	.51
E1-2	11 10 41.4	-76 16 22	11.48	.76	.14	4/79	B	-	e	.24
E1-4	11 11 49.7	-76 18 03	9.67	.78	.21	4/79	B	-	e	.27
E1-5	11 10 33.7	-76 18 24	10.07	.78	.38	4/79	M	S 40	d,e	
E1-6	11 11 55.9	-76 19 23	10.75	.69	.31	4/79	M	S 44	e	
E1-7	11 09 58.5	-76 20 09	9.86	.86	.27	4/79	B	-	e	.39
E1-8	11 11 06.3	-76 20 51	9.27	.68	.14	4/79	B	-	e	.12
E1-9b	11 10 51.0	-76 20 47	8.59	.81	.17	4/79	B	-	d,e	.10
E1-9a	11 10 48.2	-76 20 53	8.17	.79	.46	4/79	M	S 41	d,e	
E1-10	11 10 27.4	-76 20 46	10.82	.71	.34	4/79	B?	-	e	

Table 2 – *continued*

SOURCE	RA (1950)	DEC	K	J-H	H-K	DATE	(7)[a]	(8)[b]	NOTES	E(J-K)
E2-1	11 11 46.0	-76 24 07	7.52	1.07	.30	4/79	B	-	e	.71
E2-3	11 11 22.2	-76 27 23	9.18	.90	.24	4/79	B	-	e	.45
E2-4	11 10 52.5	-76 28 09	6.74	.95	.67	4/79	M	H 30	d,e	
E2-5	11 11 14.2	-76 28 07	11.29	.90	.24	4/79	B	-	e	.45
E2-6	11 10 36.6	-76 28 46	11.69	1.17	.27	4/79	B	-	e	.86
E2-7	11 11 36.7	-76 29 24	11.21	.94	.24	4/79	B	-	e	.51
E2-8	11 10 09.4	-76 29 39	9.64	1.23	.38	4/79	B	-	e	.95
E2-9	11 11 13.1	-76 30 53	11.20	.70	.28	4/79	B?	-	e	
E2-10	11 11 35.9	-76 31 26	10.23	1.01	.27	4/79	B	-	e	.62
E2-11	11 10 12.9	-76 31 33	11.42	.87	.36	4/79	B	-	e	
E3-1	11 11 05.1	-76 34 26	10.26	.95	.25	4/79	B	-	e	.53
E3-2	11 10 29.8	-76 34 42	10.43	.84	.28	4/79	B	-	e	.36
E3-3	11 09 36.9	-76 35 38	10.85	1.63	.74	4/79	B	-	e	1.55
E3-4	11 10 18.5	-76 35 47	10.52	1.67	.66	4/79	B	-	e	1.61
E3-5	11 09 38.3	-76 41 08	8.66	1.28	.44	4/79	B	= C3-2	e	1.02
E3-6	11 11 15.7	-76 41 30	11.24	.59	.29	4/79	B?	-	e	
E4-2	11 10 37.9	-76 41 54	11.15	.66	.30	4/79	B	-	d,e	.84
E4-3	11 11 08.5	-76 42 26	9.50	.75	.19	4/79	B	-	e	.23
E4-4	11 11 45.8	-76 44 50	9.97	.78	.22	4/79	B	-	e	.27
E4-6	11 10 40.4	-76 49 11	11.60	1.36	.46	4/79	B	-	e	1.14
E4-7	11 09 51.4	-76 49 42	10.71	.87	.31	4/79	B	-	e	.41
E4-8	11 12 15.7	-76 50 26	9.30	.95	.22	4/79	B	-	e	.53

a B = Background Field, M = Member

b H = Henize and Mendoza (1972), S = Schwartz (1977)

c CVF Spectra

d Optical Spectra

e Coordinates Good to ± 5"

f Coordinates Good to ± 10"

2.4 OPTICAL SPECTROSCOPY

In order to examine the nature of some ambiguous objects, i.e., those which are not clearly associated with the cloud, nor which are easily identified as field stars, optical spectra of 10 sources were obtained. The spectra covered the wavelength region λ 4000–5000 Å, and were acquired using the photon counting array (Stapinski, Rodgers & Ellis 1979) attached to the Cassegrain spectrograph of the Mt Stromlo Observatory 1.9-m telescope. The resolution of the system was 3 Å, and was clearly sufficient for our spectral classification needs.

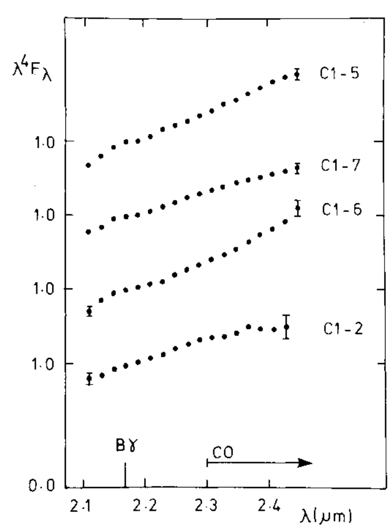

Figure 1. Low resolution ($\lambda/\Delta\lambda \sim 50$) spectra of four cloud members with IR excesses.

Table 3. Optical spectra.

Source	Spectrum
C1–5, H23	em.
C1–7, WWCha	em.
C1–9	no em.
C4–2	G5
C6–1, H20	em.
E1–5, S40	K0 em.
E1–9a, S41?	K0 em.
E1–9b	G8 III
E2–4, H30	G8 V em.
E4–2	F

Objects for which spectra were obtained, together with notes on their spectra, are listed in Table 3. The group includes six known emission-line stars, and our spectra confirm the presence of emission in each case at the time of our observation. Four objects, for which no previous spectroscopic data exist, were found to have spectra lying in the range F5–G8. None of these exhibited emission at the time of our observations, and are probably all background field stars.

3 The population of background objects

3.1 DISCRIMINATION BETWEEN BACKGROUND AND CLOUD MEMBERS

A most important aspect of the study of star formation within dark clouds is the discrimination of the background field stars from the sources associated with the cloud itself. Although the effect of confusion by background objects is minimized in Chamaeleon by the location of the cloud out of the galactic plane (l = 297°, b = – 15°), it is nevertheless still important. Elias (1978a, b) was the first to realise the importance of such contamination in his studies of IC 5146 and the Taurus and Ophiucus dark cloud complexes. His measurements went only as faint as $K = 7$, so that for the present study of Chamaeleon, reaching as it does to magnitudes in the range $K = 10$–11, the problem of contamination becomes acute.

Galactic model predictions (Jones *et al.* 1981) for the Chamaeleon region demonstrate the importance of old disc field stars, as one scans to fainter K magnitudes. A plot of the model predictions at the galactic coordinates of Chamaeleon for the number of stars per square degree down to a given K magnitude is given in Fig. 2, where it is compared with the

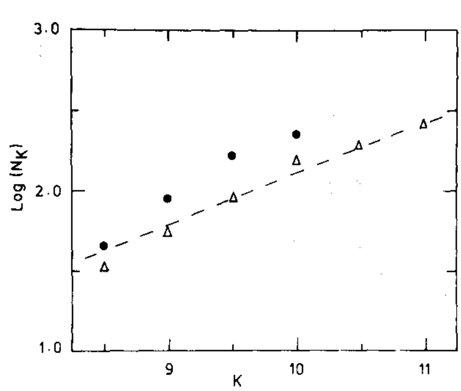

Figure 2. The 2.2 μm (K) luminosity function of the eastern blocks (open triangles) and the northern four central blocks (filled circles).

observations of the eastern blocks lying on the edge of the dense cloud region. The agreement of the predictions with the model for this area emphasizes the importance of the background component, and suggests that in the eastern blocks at least, association objects should comprise no more than ~ 25 per cent of the observed stars.

However, despite the difficulties engendered by the presence of background objects, there are several means of discriminating individual cloud members from that population which, taken together, provide an almost 100 per cent effective approach. These are:

(a) The presence of T Tauri-like emission lines in the optical spectra of sources, which is a sure sign of their membership of the clouds. This is the historical method for the discovery of pre-main-sequence objects, and has been applied successfully to the Chamaeleon region by Henize & Mendoza (1973), Schwartz (1977) and Appenzeller (1977, 1979).

(b) Infrared spectroscopy in the 2–2.4 μm region, which was successfully used by Elias (1978a, b) to discriminate between association and field star sources in the Taurus and Ophiucus dark cloud complexes. His approach was to identify any source with strong CO absorption (indicative of a late-type giant) as a background object and those with smooth spectra (because they were early-type dwarfs or had strong dust continua) as cloud members.

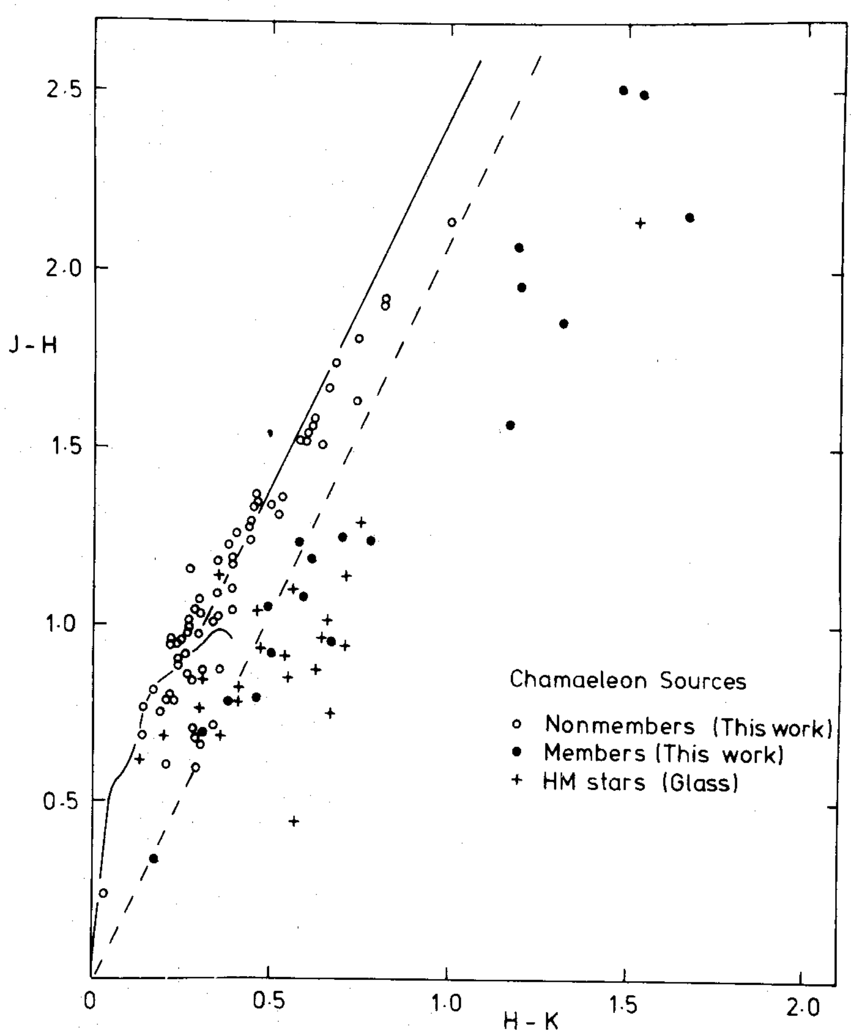

Figure 3. The *JHK* colours of all of the objects in Table 2, and of the HM emission line stars observed by Glass (1979) that are not in common with those in Table 2. The curved solid line is the intrinsic sequence for field giants.

Although this approach is very successful it is also time consuming and is not a feasible approach for the very faintest sources.

(c) It has been shown empirically by Hyland (1980) that the *JHK* data available for the Taurus and Oph dark cloud complexes (Elias 1978a, b) and for the optical sources in Chamaeleon (Glass 1979) is extremely efficient in discriminating between cloud members and background objects. In a $(J–H)$ versus $(H–K)$ plot, the cloud members can be identified by their $(H–K)$ excesses, while the field stars follow a tight locus along an interstellar reddening curve from the region of intrinsic colours of K and M giants.

In this paper we use all three techniques to shed light on the nature of individual sources in the Chamaeleon region. In the first instance we use the $(J–H)$ versus $(H–K)$ diagram to make an initial selection of the background stars and cloud members. This diagram (on the AAT system) for all measured Chamaeleon sources (including the emission-line objects measured by Glass 1979) is shown in Fig. 3. The observed values are compared with (i) the intrinsic giant colours and (ii) interstellar reddening trajectories (see Jones & Hyland 1980), for both late-type giants (solid line) and early-type (A) stars (dashed line). Several interesting features may be noted in this figure: (a) a large population of background field stars stretches along the near-infrared reddening trajectory for giants in a manner analagous to the Taurus and Coalsack dark cloud complex (Jones *et al.* 1980); (b) a clear set of excess $(H–K)$ objects (which may be identified as cloud members) follows the locus of similar objects in Taurus. Any source to the right of the dashed line may be unambiguously assigned to membership within the cloud; (c) there is a significant group of ambiguous objects clustered in the vicinity of $(J–H) \approx 0.7$, $(H–K) \approx 0.3$. Such a population is absent from the similar figure for the Coalsack region (Jones *et al.* 1980), which appears to contain only background giants. Spectroscopic observations of a few of these (Schwartz 1977) confirmed by our own data (Section 2), reveal weak Balmer emission, suggesting that a significant fraction of these may be pre-main-sequence objects with less extreme shell characteristics. The CVF spectra and optical spectra described in Section 2 were used in doubtful cases to confirm and aid the final discrimination.

It is important, however, to estimate the expected fraction of field stars present in this ambiguous portion of the colour–colour plot. The field stars that can occupy this portion of the diagram are M dwarfs, and reddened B–F5 stars with $E(J–K) \sim 1.0$. Stars with spectral types intermediate between these groups would have colours to the left of this distribution. For the completed northern seven central blocks (complete to $K = +10.5$) one would expect about two B–F5 background stars and about one M dwarf foreground star according to the Jones *et al.* model. For the eastern block (complete to $K \sim 11.5$) the corresponding numbers are three and two. However, there is not enough extinction in the eastern blocks [$0.0 < E(J–K) < 0.9$, see Section 3.3] to redden randomly distributed background B–F5 stars to the colours of the group of sources in question. Thus, one would expect ~ 5 field stars to lie in the vicinity of $J–H \sim 0.7$, $H–K \sim 0.35$ in Fig. 3. There are six stars in Table 1 which have these colours but have not been identified as emission-line objects by Henize & Mendoza (1973) or Schwartz (1977). Two have non-emission spectra (Table 3). As a consequence we will identify the remaining four sources as non-members from a *statistical* standpoint, even though one or more may be members. These sources are indicated by a B? in column 7 of Table 2.

The CVF spectra of the extremely red sources C1–5, C1–7, C1–6, C1–2, all showed the expected smooth continuum (Fig. 1), similar to the spectra of embedded sources in Taurus (Elias 1978). The spectra show possible evidence for Brackett γ emission at 2.16 μm for C1–5, 6, 7 and C1–2 may show small CO band absorption on top of the thermal continuum. It would appear that the latter object is likely to be a member of the dark cloud

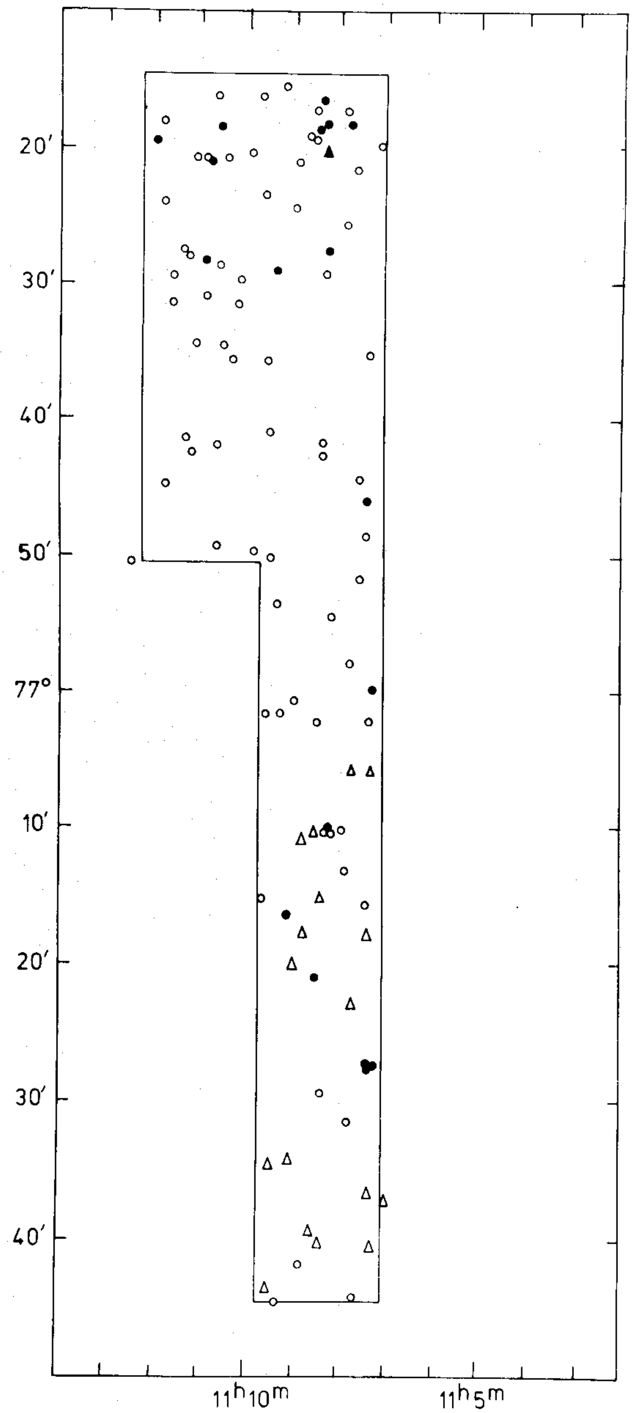

Figure 4. The spatial distribution of the sources found in the 2 μm scans. Circles indicate sources that have been measured photometrically (Table 2), with filled circles indicating association members. Sources plotted as open triangles have not had *JHK* photometry.

complex embedded deep in the cloud because the 2 μm continuum is steeper than would be expected from interstellar reddening alone for the observed *J–H* colour.

Our adopted identification of the individual sources as dark cloud members or field stars is noted in column 7 of Table 2, and the spatial distribution of sources with identifying symbols is shown in Fig. 4. Probable association members are shown as filled circles.

3.2 INTERSTELLAR REDDENING LAW IN CHAMAELEON

The law of interstellar extinction in the vicinity of dark clouds is extremely important for the determination of distances to the clouds, and for determining the intrinsic energy distributions of embedded sources. There is considerable controversy in the literature regarding the value of R to be used within such regions, and current thinking on this matter has been briefly summarized by Hyland (1980).

In the Chamaeleon dark cloud complex, a knowledge of the reddening law is crucial for the determination of the distance to the cloud. Grasdalen *et al.* (1975) derived a value of $R = 5.6$, from optical and infrared observations of HD 97300. This B9 V star, the illuminating source for the reflection nebula Cederblad 112, is the generally used distance calibrator. With the above value of R, the distance to Chamaeleon becomes 110 pc, and (in contrast to the results of Cohen & Kuhi 1977) many of the young emission-line stars fall below the main sequence. Rydgren (1980) adopted a somewhat smaller value of R (= 5.0), but cautions against the use of such a value, derived as it is from HD 97300. This star is young, associated with the dark cloud complex and may very well possess a circumstellar shell.

Indeed, in Fig. 5 reddening ratios $E(V-\lambda)/E(B-V)$ derived for HD 97300 are compared with (a) the normal reddening curve (dashed line) and (b) a curve derived by assuming that a normal ($R = 3.0$) reddening law applies, and that HD 97300 consists of a B9 V star plus a 3000 K blackbody component (solid line). It can be seen that the addition of a blackbody component satisfactorily fits the observed data without recourse to large values of R. If such a component were to be the correct explanation, two alternative interpretations are possible: (a) the extra component may be a pre-main-sequence M star companion to HD 97300 with $M_{bol} \approx 3.8$ or (b) it may be a hot ($T \sim 3000$ K) optically thin dust shell. The latter interpretation is difficult to accept since such hot dust shells are virtually unknown and unexpected, because of the evaporation of the dust particles at lower temperatures. Note that a lower temperature shell will still reduce the value of R; however, interpretation (a) is more favourable, and can be tested in future by high-resolution spectroscopy in the 2 μm region.

In the light of the problems encountered by use of a large value of R in the interpretation of HD 97300, and the fact that plausible alternative explanations exist for its peculiar near

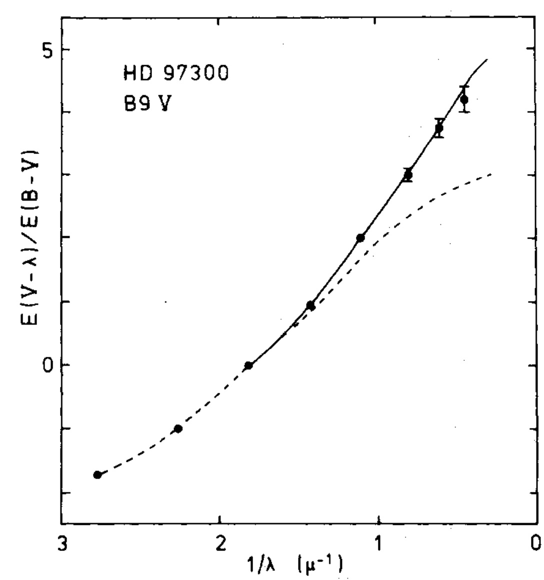

Figure 5. The colour excess ratios for HD 97300 (filled circles). The dotted curve is the normal interstellar reddening curve. The solid curve shows the effect of adding a 3000 K blackbody.

infrared colours, we have adopted $R = 3.1$, and estimate that the cloud is 215 pc distant. This value is used for all following discussion.

Regardless of the extinction law applicable to HD 97300, the background sources identified in the previous section follow the same near-infrared interstellar reddening trajectory (Fig. 3) as sources in the Coalsack, and near the Galactic Centre (Jones *et al.* 1980; Jones & Hyland 1980). These results strengthen the conclusions of other workers (Elias 1978a, b; Glass & Penston 1975; Glass 1979) that the *near-infrared* reddening law in dark cloud regions as obtained from background stars is entirely normal.

3.3 DISTRIBUTION OF EXTINCTION WITHIN THE CHAMAELEON DARK CLOUD

The sources identified as background field stars are evenly and randomly distributed over the survey area. The colours of these sources have thus been used to define the distribution of extinction within the cloud. It was only possible to do this satisfactorily for the area north of $-77°$, where our photometric coverage of the sources was complete. This approach provides details of the cloud structure into the densest regions which are not amenable to

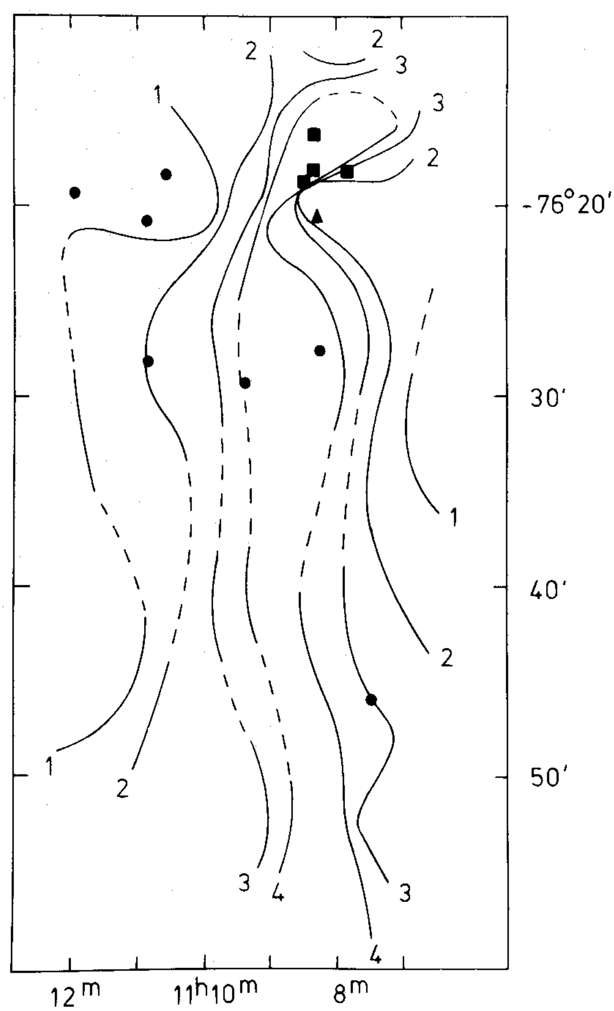

Figure 6. The distribution of extinction in the northern eight blocks based on photometry of the background field. The lowest contour (1) is $E(J-K) = 0.4$ ($A_V = 2.5$) and the contour interval is $E(J-K = 0.25$ ($A_V = 1.56$). Association members with strong IR excesses are indicated by filled squares, those with mild IR colours by filled circles. The location of HD 97300 is shown as a filled triangle.

optical study. It can also be used (see Section 4) to provide an estimate of the interstellar component of extinction to source embedded within the cloud.

Values of $E(J-K)$ for individual background sources were derived as follows: (a) by adoption of intrinsic colours for the object if spectral information was available, or (b) by adopting intrinsic colours of giants as being representative of the mean background stellar population (~ G8 III). For a few apparently early-type stars an approximate value of $E(J-K)$ was obtained by projecting the colours of the object back along a reddening trajectory until it merged with the intrinsic colour line. The results of applying these procedures to the individual sources are given in column 10 of Table 2. From these, a contour map of the extinction $E(J-K)$ was constructed for the northern region of our study (Fig. 6). This map clearly shows the elongated structure of the cloud, reaching a central extinction of $E(J-K) \approx 1.15$ along its length, corresponding to a relatively modest $A_V \sim 7$. It also exhibits an interesting steep gradient of extinction just north of HD 97300 which will be discussed further in Section 4.

4 The population of cloud members

4.1 SPATIAL AND MAGNITUDE DISTRIBUTION

Inspection of Plate 1 and Figs 4 and 6 shows that those sources identified as cloud members exhibit a tendency to be associated with those cloud regions of highest extinction. The significance of this result becomes apparent when the magnitude distribution of the sources is taken into account (and remembering that the limiting magnitude of the survey was approximately 1 mag fainter for the eastern blocks than for the central high-extinction region).

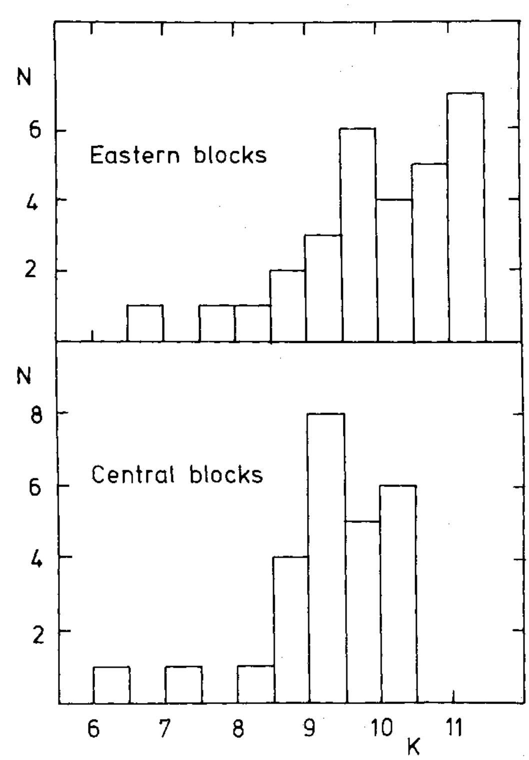

Figure 7. A histogram of the K magnitude distribution for the eastern blocks (top) and the four northern central blocks (bottom). The eastern blocks were surveyed to $K = 11.5$, the central blocks to only $K = 10.5$.

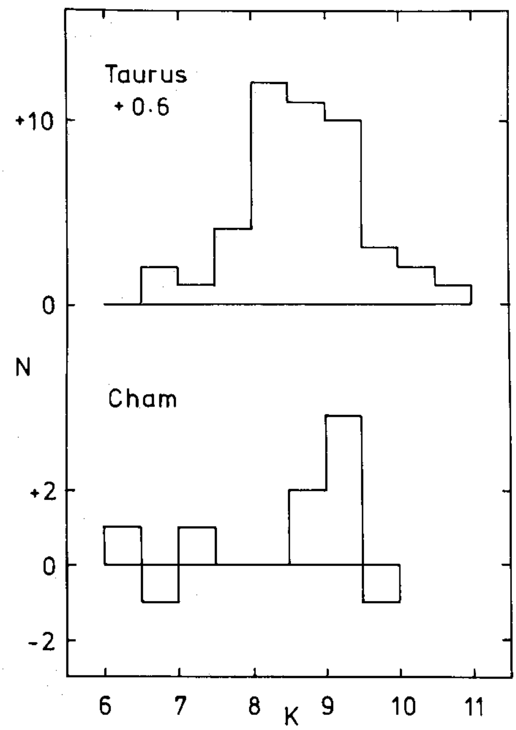

Figure 8. A comparison of the K luminosity distribution of the Taurus dark cloud and the difference between the two K distributions in Fig. 7 for the Chamaeleon.

Fig. 7 shows the magnitude–number distribution for all sources within the central blocks number 1–4, and the contiguous eastern blocks, an effect which would be enhanced by correcting for extinction.

Statistically the effect is easily seen in the luminosity function plot for the two areas (Fig. 2). As mentioned above, the observed luminosity function for the eastern blocks is fitted remarkably well by the galaxy model predictions of Jones *et al.* (1981). The central blocks, however, have a significant excess of sources in the magnitude range $7 < K < 9$. The excess of sources in the central regions as a function of K magnitude is plotted in Fig. 8, and is compared there with the K magnitude distribution of optically chosen members of the Taurus dark cloud complex (Cohen & Kuhi 1979), corrected so as to be at the distance adopted for Chamaeleon.

Although the number of Chamaeleon sources is not large, the distributions are similar. There is the suggestion that Chamaeleon is deficient in bright sources compared with Taurus. It is worth noting that if the distance to Chamaeleon were to be decreased to ~ 120 pc, as suggested by Grasdalen *et al.* (1975) using $R = 5.5$, the Chamaeleon sources would be significantly fainter than those of Taurus. It is clear that an independent distance indicator for the Chamaeleon dark cloud is urgently required. At the same time, a deep survey of the Taurus region is needed to delineate the faint end of the magnitude distribution, since it would appear that the IR survey of Elias was not deep enough to have revealed all possible member sources.

The above approach is purely statistical; it does not take into account indicators of cloud membership as applied in Section 3, and merely serves to strengthen the notion that a significant population of pre-main-sequence cloud members lies in the central obscured region of the cloud. The fact that these are among the brightest cloud members also suggests that the *youngest* sources are to be found within the densest regions.

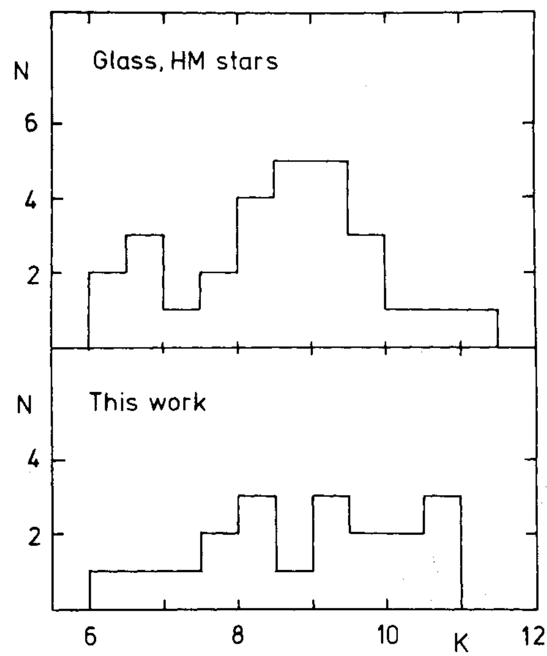

Figure 9. A histogram of the K magnitude distribution for association members based on optical surveys (top; Glass 1979) and the infrared survey (bottom).

A re-examination of the magnitude distribution of identified cloud members determined by the present survey is shown in Fig. 9, where this distribution is compared with the purely optical sample of Henize & Mendoza (1973) from a much larger region. This comparison serves to show that the K magnitude distribution, although similar to the sample of optical emission-line stars, has a greater percentage of stars at magnitudes fainter than 10. It may be confidently inferred from this comparison that the optically defined sample of emission-line stars in dark cloud regions is magnitude limited. Our Chamaeleon sample shows that there is a sizeable number of lower luminosity sources present, and that even fainter ones may also be members but have yet to be identified. The luminosity function at the low luminosity end still needs delineating and may be dependent upon the age of the complex.

4.2 SMALL-SCALE CLUSTERING

Examination of the spatial distribution of cloud members within our survey region reveals the presence of at least two small centres of clustering at $11^h 08^m$, $-76° 18'$ and $11^h 07^m$, $-77° 28'$. Both of these small groups of members lie adjacent to a sharp density increase in the cloud which in turn is adjacent to one of the bright early-type stars associated with the complex (HD 97300, 97048). The morphology of these regions is suggestive of density compression at the edge of dense cloud regions (possibly causally related to the young early-type stars), in which a group of very young low mass objects had formed. Detailed structure of the cloud around the southern group is not known, and further and deeper observations are required. For the northern cluster, however, the extinction map (Fig. 4) is clearly suggestive of a compression of the cloud by HD 97300 which presumably has ended its T Tauri phase and has cleared away most of the cloud material from its immediate vicinity. This may represent the clump coalescence and compression phase in the model for low mass star formation developed by Norman & Silk (1980).

4.3 THE EFFICIENCY OF STAR FORMATION IN THE CLOUD

An important aspect of the present study has been to evaluate the success of $2\,\mu m$ surveys in revealing dark cloud members embedded deep within the cloud and thus *optically* unrecognizable. On the basis of the division of survey sources into background field stars and cloud members, some nine previously undiscovered (or unrecognized) sources have been added to the list of Chamaeleon complex members. Four of these have strong infrared excesses and are clearly deeply embedded within the cloud and/or thick circumstellar dust shells. The remaining five do not possess such extreme colours and from their K magnitudes are possibly lower luminosity members of the cloud with weak or absent emission lines. These may in fact be objects which have almost completed their evolution towards the main sequence and have entered a quiescent phase producing little line emission.

This list of additional members nearly doubles the number of previously known emission line objects (10) within the area of the survey, and may yet need to be increased further when photometry of all sources in the southern blocks has been completed. It is thus clear that $2\,\mu m$ surveys of this kind provide a sound technique for probing the depths of young dark cloud regions when due consideration is given to confusion. The significant increase in probable cloud members revealed by the present study has implications with regard to the efficiency of star formation.

Rydgren (1980) estimated the star formation efficiency (i.e. the percentage of cloud mass which ends up as stars) within the entire Chamaeleon dark cloud complex to be ~ 8 per cent. This was done by using star counts to estimate the distribution of A_V and then converting A_V into molecular hydrogen column densities. The total mass of the cloud ($670 M_\odot$) was then compared to the total number of known emission-line stars in the region (Schwartz 1977) with the assumption of $\sim 1\,M_\odot$ each. (See Cohen & Kuhi 1979 for a more realistic mass spectrum.) It is interesting to note that a major fraction of the emission-line objects is *outside* the most highly obscured areas. Whether or not these stars formed out of the presently visible dark material and due to random peculiar velocities separated from these regions, or actually formed in dense material that has by now been dissipated is not clear. Since a relative projected motion of only $1\,km\,s^{-1}$ would move a star ~ 15 arcmin in 10^6 yr at the distance of the Chamaeleon, the first possibility is quite reasonable.

An estimate of the mass in the northern blocks can be obtained from the extinction map (Fig. 6) by a method detailed in Jones *et al.* (1980) for the Coalsack, and a value of $\sim 200\,M_\odot$ is obtained. Extrapolating this mass to the rest of the dark material visible on photographs yields $\sim 700\,M_\odot$ for the entire cloud, compatible with Rydgren. For the highly obscured northern four central blocks, the cloud mass is $\sim 140\,M_\odot$. There are at least eight member stars within these blocks (see Section 4.1), corresponding to a minimum of $\sim 10\,M_\odot$ ($\sim 3\,M_\odot$ for HD 97300, A0 V). Thus, within the *densest regions alone,* the star formation efficiency is ~ 7 per cent or greater.

As mentioned in this section, we have identified nine new members in the central blocks that were too red to be visible on survey plates. Since the central blocks were surveyed to only $K \sim 10.5$, and blocks C8 through C10 had incomplete photometry, the actual number is certainly greater. Taking this into consideration, and extrapolating these numbers to the rest of the dark material (~ factor of 2) increases the efficiency of star formation of the *entire dark cloud* (not just small selected regions, see Cohen & Kuhi 1979) by at least a factor of 1.5 to a value of ~ 12 per cent.

The presence of 'hidden' association members is probably not unique to the Chamaeleon dark cloud. In all likelihood, deep $2\,\mu m$ surveys would reveal similar numbers of pre-main-sequence stars in other well-studied dark clouds that have used optical surveys (Cohen & Kuhi 1979) or infrared surveys that do not go deep enough (Elias 1978a, b, c). Thus, we conclude that the actual star formation efficiency in dark cloud T Tauri associations is greater than previous calculations would indicate.

4.4 ENERGETICS AND STAR FORMATION IN THE CLOUD

Considerable evidence has accumulated that dense molecular clouds may possess complex velocity fields. One possible explanation is that the observed molecular linewidths are due to systematic motions on a large scale, such as radial infall (Goldreich & Kwan 1974) or rotation (Field 1978). An alternative explanation is that a more complex velocity and density structure on smaller scales is necessary to explain the observed line profiles. Norman & Silk (1980) have proposed such a clumpy cloud model in which the energetics of the intercloud medium is driven by the stellar winds of numerous low mass PMS stars. In this model, the winds from T Tauri stars form bubbles inside the cloud. These bubbles eventually intersect, forming density clumps that coalesce into new T Tauri stars. That is, T Tauri star formation may be self-sustaining if the swept-up matter forms clumps that are Jeans unstable. These clumps experience dissipative effects, however, and there must be sufficient T Tauri stars ($\sim 10\,pc^{-3}$) to maintain the process, otherwise leakage occurring in the clumps will restore the gas to a more homogeneous and quiescent state. Thus, a major requirement of the Normal & Silk model is the presence of a high space density of PMS objects in dark cloud/T Tauri associations.

Norman & Silk are principally concerned with more massive clouds ($\sim 10^4 M_\odot$) than the Chamaeleon ($\sim 10^3 M_\odot$). None the less it is important to compare their model predictions (which assume only low mass star formation is taking place) with our results for the Chamaeleon, a dark cloud which clearly is not producing massive stars, and is probably of intermediate age (see Section 5). If the cloud is taken to be as thick in the line-of-sight as it is wide (~ 9 arcmin or 0.56 pc), then the volume of the central 10 blocks corresponds to $\sim 1.7\,pc^3$. Our survey has found a total of 14 PMS stars in the central blocks (not counting HD 97300) corresponding to a space density of $\sim 8\,pc^{-3}$ remarkably close to that required by Norman & Silk. As pointed out in Section 4.3, there are certainly more cloud members yet to be found in this area, so the value of $8\,pc^{-3}$ is a *lower limit* only. Note that this calculation applies to the *entire* cloud within the central blocks, not just selected areas of high member concentration. Clearly, the conclusion in Section 4.2 that all dark clouds have a higher concentration of PMS stars than previously thought may bear directly on the energetics and small-scale structure of those clouds.

In Section 4.2 it was suggested that a compression of the cloud had taken place to the north-east of HD 97300. It is tempting to associate this arc of steep density gradient as the remnant of a bubble formed by the wind in an earlier T Tauri phase of HD 97300. It is important that the four PMS stars near this arc, are probably very young, as indicated by their strong IR excesses. The formation of these four stars may have been a direct result of the stellar wind from HD 97300 and they, in turn, may continue the process with their own winds.

5 Interpretation of the continua of association members

In previous sections of this paper we have identified a group of 'association members', the large majority of which should be pre-main-sequence objects. One of the clearest discriminators of these members was the presence of an intrinsic infrared excess in the $J-H$ versus $H-K$ plane, similar in character to those exhibited by embedded sources in the Taurus, Oph and RCr A dark clouds (Elias 1978b, c; Glass & Penston 1975). The source of these intrinsic excesses is usually discussed in terms of free–free radiation or thermal dust emission. While it is conceivable that both mechanisms contribute to the excesses observed in T Tauris and other PMS objects, there is considerable evidence to favour the latter over the former. Cohen & Kuhi (1979), in a comprehensive study of several dark cloud T associations, concluded that dust emission alone provides a satisfactory representation of the observed properties of the PMS objects. While emission from a hot (~ 10^4 K) chromospheric shell is able to provide an adequate explanation for a number of less extreme cases, many objects could only be interpreted in terms of a thermal dust continuum. Clearly an argument for ubiquitous dust emission is tenable.

In this investigation we have the opportunity to evaluate the success of circumstellar shell dust models as they apply to a large sample of PMS objects within the same region. As for previous studies, however, the confusing effects of interstellar reddening within the cloud play a major role in determining the observed stellar colours. In the following paragraphs, we make the first serious attempt to derive intrinsic colours for the sources, for direct comparison with theoretical models.

5.1 DERIVATION OF INTRINSIC COLOURS

Two widely differing methods have been used in deriving final colours for the sources. The first makes use of the extinction map (Fig. 4) derived earlier from observations of field stars behind the dark cloud. From this map, extinction $E(J-K)$ for each individual embedded member source was obtained on the assumption that each source was 0.6 of the way through the cloud. This plausible assumption produced the best agreement with the second method of extinction derivation for objects common to both techniques.

The second method was applied to those objects with measured optical colours as well (notably those from the HM list measured in the IR by Glass). Initial estimates for $E(V-K)$ [designated $E(V-K)_I$] were obtained on the assumption that $(V-K)_0 \sim 2.0$ for all the sources. This assumption is an upper limit for $E(V-K)$, since it does not take into account the possible effects of dust shell emission. If these sources are dereddened along the interstellar reddening line in a $J-H$ versus $V-K$ plot, they cross $V-K = 2.0$ at $J-H$ colours *redder* than the intrinsic $J-H$ colours for G, K and M dwarfs. This, as expected, is due to the presence of a dust shell. If one uses a crude estimate of the locus in a $J-H$ versus $V-K$ plot due to the addition of dust emission to late-type dwarfs (as derived from the models described later), it is found that dereddening to this line (rather than all the way to $V-K = 2.0$) on average gives $E(V-K) = 0.75\,E(V-K)_I$. This revised $E(V-K)$ could then be used to obtain $E(J-K)$ [$= 0.2\,E(V-K)$; Lee 1970].

The derived intrinsic *JHK* colours are listed in Table 4 and plotted in Fig. 10. Recognizing that these intrinsic colours are still subject to a fair degree of uncertainty, especially for the most deeply embedded sources, with large values of $(J-H)_0$ (i.e. > 1.5), we are now in a position to compare them with theoretical dust shell models.

5.2 CIRCUMSTELLAR DUST SHELL MODELS FOR PMS OBJECTS

For this program we have constructed a number of circumstellar dust shell models aimed at representing the continua of PMS sources in Chamaeleon.

The model, based on the 'quasi-diffusion' method of Leung (1975, 1976), has been described by Mitchell & Robinson (1978) and Mitchell (1979). In the model the differential form of the radiative transfer problem in an extended circumstellar dust shell is solved numerically.

Table 4. Intrinsic colours of association members.

HM	HJM	Other	$(J-H)_0$	$(H-K)_0$
1	–	SX Cha	0.67	0.50
2	–	SY Cha	0.73	0.37
3	–	TW Cha	0.69	0.50
4	–	LH_α 332–20	0.62	0.33
5	–	–	0.47	0.41
7	–	–	0.55	0.14
8	–	–	0.43	0.14
9	–	–	0.70	0.44
11	–	VY Cha	0.23	– 0.05
12	–	–	0.88	0.23
13	–	CD–76 486	0.70	0.60
14	–	VV Cha	0.55	0.29
15	–	–	0.91	0.57
16	–	–	1.69	1.31
17	–	VW Cha	0.79	0.54
18	–	HD 97048	0.24	0.47
19	–	–	0.59	0.19
20	C6–1	–	0.76	0.47
21	C4–5	VY Cha	0.87	0.61
22	–	VZ Cha	0.10	0.55
23	C1–5	–	1.67	1.44
24	C1–7	WW Cha	1.08	0.94
25	C8–3	–	0.72	0.42
26	–	WY Cha	0.84	0.43
28	–	WZ Cha	0.62	0.44
29	–	XX Cha	0.59	0.49
30	E2–4	LH_α 332–21	0.69	0.55
–	C1–2	–	2.02	1.25
–	C1–6	–	2.13	1.37
–	C1–11	HD 97300	0.13	0.08
–	C2–3	–	0.70	0.38
–	C2–5	–	0.43	0.27
–	C7–1	–	0.83	0.39
–	C7–11	–	0.69	0.32
–	C9–1	–	1.37	1.09
–	C9–2	–	1.47	0.97
–	C9–3	–	1.58	0.96
–	E1–5	S40	0.62	0.30
–	E1–6	S44	0.69	0.31
–	E1–9a	S41	0.63	0.38

Before discussing the actual models presented, it is important to place parametric constraints on the Chamaeleon PMS objects and their dust envelopes. The intrinsic spectral types of the heavily obscured sources are difficult to determine since no visible objects are apparent, by contrast with the T-association sources discussed by Cohen & Kuhi. In their work, statistical grouping around a mean spectral type is seen within individual associations, and is clearly due to evolutionary status. We have chosen to adopt a representative spectral–luminosity range of G8 IV to K5 IV for the Chamaeleon objects, in view of the presence of HM objects with small $H-K$ excesses just redward of the locus resulting from this choice. Too late an intrinsic spectral type would render these stars difficult to interpret.

The dust opacity has been modelled on the basis of a three-component mixture of forsterite (Mg_2SiO_4), graphite and silicon carbide particles averaged over size distributions with rms radii 0.1, 0.05 and 0.05 μm respectively, as employed by Mitchell & Robinson

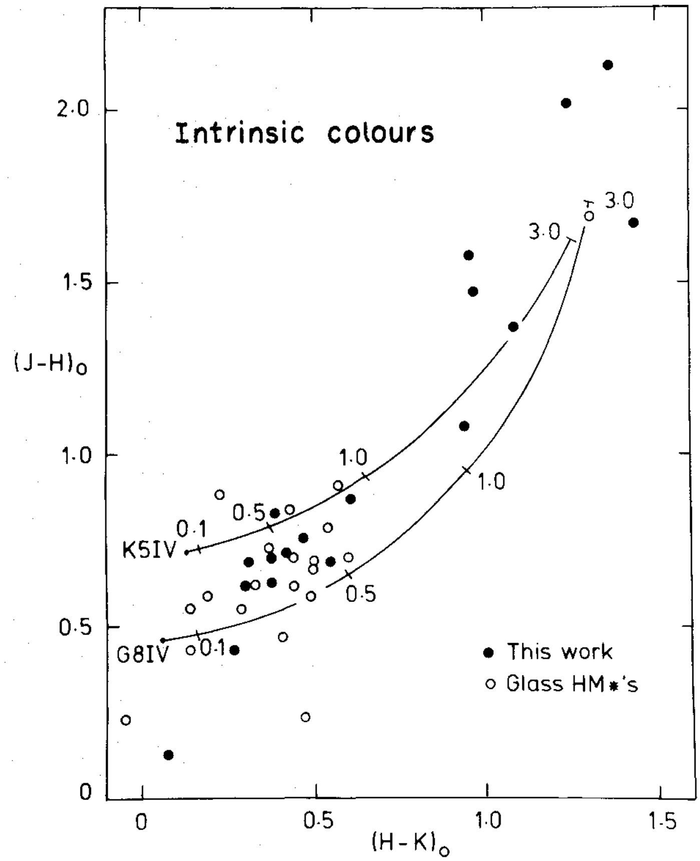

Figure 10. The dereddened *JHK* colours for the association members. The two dust shell model curves are described in the text.

(1978, 1981). The number fractions of the three components are 0.45, 0.50 and 0.05 respectively. This mixture is based on the study of Kunkle (1981), who found a similar multi-component mixture necessary to match the interstellar extinction curve from 0.12 to 4.0 μm.

The dust density distribution ideally should be tied to a dynamical collapse model for the evolving protostars. The analysis of Larson (1969) suggests a power law of the form $\rho = \rho_0 r^n$ where $n \approx -1.5$. We have adopted a slightly flatter law, $n = -1$, since the association of far-infrared excesses with some Tauri objects (Harvey, Thronson & Gatley 1979) indicates the need for significant quantities of dust at a large distance from the star.

Sample model results for a central star with $T = 5400$ K (~ G8) are given in Table 5 for a maximum shell radius of $10^3 R_*$ and in Table 6 for a maximum shell radius of $10^5 R_*$. The models in Table 5 are plotted in Fig. 11 along with the model results for the $R_{min}/R_* = 25$ case for a 4400 K (~ K5) central star. The lines shown represent sequences of increasing optical depth at 1 μm from the inner to outer shell boundaries. Models B and D in Fig. 11 are also plotted in Fig. 10. It can be seen from Fig. 10 that the G8 IV and K5 IV models with $R_{max}/R_* = 10^3$ and $R_{min}/R_* \sim 25$ provide a most satisfactory basis for the interpretation of the observed infrared excesses. The circumstellar extinction optical depths at 1 μm required by this interpretation are in general small, ranging from 0.1 to 1 for the large majority of sources. For only 7 objects out of 44 is an optically thick ($\tau_{1\mu} > 1$) shell demanded. These are all sources found within the densest regions of the cloud, and consequently their interstellar extinction component may have been underestimated. Nevertheless, optical depth values between 1 and 3 seem to be indicated, and are not unreasonable. The available L(3.5 μm) data are too sparse and of insufficient quality to make the statistical type of comparison in Fig. 10.

Table 5. Example dust shell models $T_* = 5400\,K$, $R_{max}/R_* = 10^3$.

$\tau_{1\,\mu m}$	R_{min}/R_*	$V-R$	$R-I$	$V-K$	$I-K$	$J-H$	$H-K$
0.1	10	0.62	0.47	2.01	0.91	0.52	0.21
0.5	10	0.64	0.57	2.95	1.74	0.75	0.57
1.0	10	0.78	0.75	4.08	2.55	1.01	0.78
3.0	10	1.65	1.90	8.49	4.94	1.63	1.07
0.1	25	0.63	0.48	1.95	0.84	0.48	0.16
0.5	25	0.66	0.59	2.87	1.63	0.65	0.60
1.0	25	0.80	0.78	4.17	2.59	0.95	0.95
3.0	25	1.67	1.88	8.79	5.24	1.73	1.31
0.1	50	0.63	0.48	1.92	0.81	0.47	0.14
0.5	50	0.65	0.59	2.77	1.54	0.60	0.56
1.0	50	0.81	0.80	4.09	2.48	0.83	0.95
3.0	50	1.72	1.90	8.90	5.27	1.65	1.52
5.0	50	–	–	–	–	2.30	1.83

Table 6. Example dust shell models $T_* = 5400\,K$, $R_{max}/R_* = 10^5$.

$\tau_{1\,\mu m}$	R_{min}/R_*	$V-R$	$R-I$	$V-K$	$I-K$	$J-H$	$H-K$
0.1	25	0.64	0.48	1.84	0.72	0.46	0.06
0.5	25	0.65	0.58	2.19	0.96	0.46	0.16
1.0	25	0.73	0.69	2.95	1.54	0.54	0.47
3.0	25	1.30	1.53	4.04	6.87	1.24	1.22

We note that, while the models plotted in Fig. 10 successfully explain the near infrared colours of the Chamaeleon pre-main-sequence objects, the 100 μm fluxes predicted by these are far too small to tally with the fluxes recorded for a few other T Tauri objects (Harvey *et al.* 1979). A more extended sequence of models with $R_{max}/R_* = 10^6$ was also computed (Table 6). These models have enhanced 100 μm emission, but increasing the proportion of dust at larger radii significantly reduces the excess in $H-K$ for a given shell optical depth, such that larger optical depths ($\tau_{1\mu} > 3$) are required to reproduce the observed location of

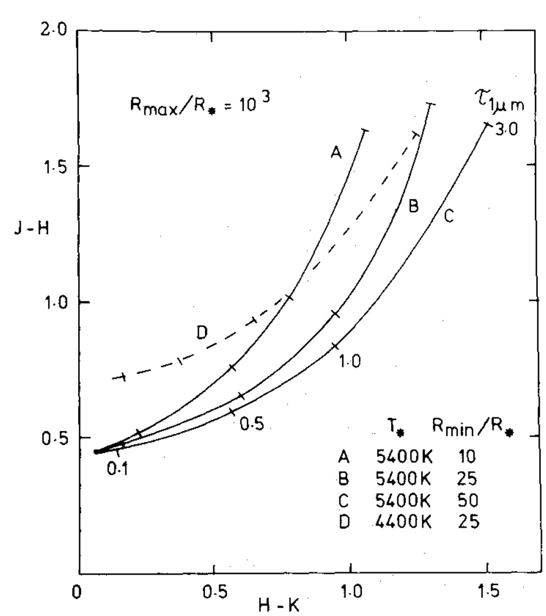

Figure 11. The *JHK* colours for a sample of dust shell models described in the text. The tick marks along the model loci correspond to the increasing shell optical depth at 1 μm.

the extreme objects in Fig. 10. Since those T Tauri stars with large far-infrared excesses are believed to have small circumstellar optical depths at 1 μm (Harvey *et al.* 1979) this may be taken as evidence for a non-continuous distribution of dust, where the near infrared flux is produced by a compact shell of maximum temperature ~ 1200 K, with the far-infrared radiation resulting from a cocoon of remnant protostellar material at much lower temperature ($T \sim 30$ K). Thus objects with only moderate excesses in the $J-H$ versus $H-K$ diagram may be strong far-infrared emitters. Far-infrared observations of a statistical sample of the PMS stars in Chamaeleon or Taurus would be extremely valuable for pursuing the general structure of such circumstellar shells.

With regard to the dust composition, it is important to note that small ($0 \sim 0.5\,\mu$m) silicate dominated mixtures are ruled out by the relatively small degree of reddening produced in the near-infrared per unit optical depth, in comparison with the graphite mixture. This is due to the comparatively small and steeply decreasing extinction of silicate dust in this wavelength region. A grain mixture containing of the order 40 to 50 per cent graphite is clearly dictated by the trajectory required to reproduce the *JHK* observations.

Finally, the success of the circumstellar model offering a consistent explanation of the near-infrared observations provides a base for a more detailed study of selected PMS objects for which more complete infrared photometry is available, and should provide important constraints on the development of dynamical collapse models.

The data exhibited in Fig. 10 also enable an estimate to be made of the distribution of the spectral types of the central stellar sources. Because of the ambiguity of $(J-H)$ values for K and M dwarfs (as can be seen from the mean dwarf line, Mould & Hyland 1976) it is not possible to make more than a crude first guess at these numbers. The assumption that all sources to the red of the M dwarf tip $(J-H) \sim 0.63$, $(H-K) \sim 0.35$ consistent with a model trajectory, are K6 or later (other than those for which optical spectral types are available) gives an upper limit to the late K and M group. We also exclude all sources redder than $(J-H) \sim 1.0$, as those cannot be uniquely matched with a dust shell model and central source. The ratio of stars earlier than G8, between G8 and K5, and later than K5 in one group, become 7:11:12, a distribution which is fairly typical of emission-line stars in the Orion complex, (12:58:39), but which appears to contain many fewer M stars than the Taurus/Auriga region (10:13:58) (Cohen & Kuhi 1979). This distribution suggests that the Chamaeleon dark cloud region may have a different mass function, or more likely is slightly older than the Taurus complex. Detailed optical and infrared spectroscopic studies are required to give a better delineation of the spectral type distribution, and HR diagram, of the association members.

6 Conclusions

In this paper we have presented the results of a 2 μm survey and subsequent photometry of a portion of the Chamaeleon dark cloud complex. The following are the major conclusions of this study.

(1) From the large number of sources revealed by the survey it has been possible on spectroscopic and photometric grounds to distinguish association members from background field stars. For the whole Cha I complex this has led to an increase of at least 50 per cent in the number of known PMS objects, resulting in a derived efficiency of star formation of > 12 per cent. It is suggested that this will be the case for other dark clouds as well.

(2) Observations of reddened background field stars evenly distributed over the region have enabled us to produce a map of the cloud extinction, and hence to infer cloud structure over a large area, including regions too dense for the presence of optical images.

(3) The data show clearly that the youngest association members are concentrated predominantly in the more dense regions of the cloud.

(4) In two cases, small clusters of PMS objects are found associated with a steep density gradient possibly caused by the interaction of the cloud with a stellar wind from a nearby early-type star. This raises the question as to whether low mass star formation may be triggered following the formation of more massive stars, in a manner mimicking the sequential star formation scenario developed for OB associations.

(5) The space density of PMS stars in the dark regions ($> 8^{-3}$ pc) and the spatial distribution of the youngest members is in good agreement with the Norman & Silk model for dark clouds.

(6) Using the extinction map in conjunction with optical and IR data on optical emission-line objects it has been possible to determine the intrinsic infrared colours of the PMS objects. These all exhibit infrared excesses, ranging from small to extreme. The extreme, optically invisible objects comprise approximately 1/3 of the association members in the survey area.

(7) Circumstellar dust shell models have been computed for comparison with the intrinsic colours of the sources. It is shown that models with central sources lying between spectral types G8 IV and K5 IV, and with $r_{max}/r_* \sim 10^3$, $r_{min}/r_* \sim 25$ provide an excellent fit to the observed data. For the majority of sources small optical depth values ($\tau_{1\,\mu m} \sim 1$) provide an adequate representation of the data. Models which predict large 100 μm fluxes, such as have been observed for T Tauri, produce optical depth values too large at V to be acceptable for known optical emission-line objects. It is suggested that this may be evidence for a non continuous dust distribution in the shells of T Tauri-like objects.

(8) A crude estimate of the distribution of spectral types among the Chamaeleon sources suggests that the ratio of G8–K5 sources to that of K6–late M is 1 : 1. This is similar to the ratio found in the Orion complex, but markedly different from that found in Taurus, and may be accounted for by an age or mass function difference between Taurus and Chamaeleon.

References

Appenzeller, I., 1977. *Astr. Astrophys.*, **61**, 21.
Appenzeller, I., 1979. *Astr. Astrophys.*, **71**, 305.
Cohen, M. & Kuhi, L. V., 1979. *Astrophys. J. Suppl.*, **41**, 743.
Elias, J. H., 1978a. *Astrophys. J.*, **223**, 859.
Elias, J. H., 1978b. *Astrophys. J.*, **224**, 453.
Elias, J. H., 1978c. *Astrophys. J.*, **224**, 857.
Field, G. B., 1978. *Protostars and Planets*, p. 243, ed. Gehrels, T., University of Arizona Press, Tucson.
Glass, I. S., 1979. *Mon. Not. R. astr. Soc.*, **187**, 305.
Glass, I. S. & Penston, M. V., 1975. *Mon. Not. R. astr. Soc.*, **172**, 227.
Goldreich, P. & Kwan, J., 1974. *Astrophys. J.*, **189**, 441.
Grasdalen, G., Joyce, R., Knacke, R. F., Strom, S. E. & Strom, K. M., 1975. *Astr. J.*, **80**, 117.
Grasdalen, G. L., Strom, K. M. & Strom, S. E., 1973. *Astrophys. J.*, **184**, L53.
Harvey, P. M., Thronson, H. D. & Gatley, I., 1979. *Astrophys. J.*, **231**, 115.
Henize, K. G., 1963. *Astr. J.*, **68**, 280.
Henize, K. G. & Mendoza, V. E. E., 1973. *Astrophys. J.*, **180**, 115.
Hoffmeister, C., 1962. *Z. Astrophys.*, **55**, 290.
Hyland, A. R., 1980. *Infrared Astronomy*, p. 125, eds Wynn-Williams, C. G. & Cruikshank, D. P., Reidel, Dordrecht, Holland.
Jones, T. J., Ashley, M., Hyland, A. R. & Ruelas-Mayorga, A., 1981. *Mon. Not. R. astr. Soc.*, **197**, 413.
Jones, T. J. & Hyland, A. R., 1980. *Mon. Not. R. astr. Soc.*, **192**, 359.
Jones, T. J., Hyland, A. R., Robinson, G., Smith, R. & Thomas, J., 1980. *Astrophys. J.*, **242**, 132.
Kunkle, T., 1981. *PhD thesis*, University of Hawaii.
Larson, R. B., 1969. *Mon. Not. R. astr. Soc.*, **145**, 297.

Lee, T. A., 1970. *Astrophys. J.*, **162**, 217.
Leung, C. M., 1975. *Astrophys. J.*, **199**, 340.
Leung, C. M., 1976. *J. quant. Spectr. rad. Trans.*, **16**, 559.
Mitchell, R. M., 1979. *PhD thesis*, University of Melbourne.
Mitchell, R. M. & Robinson, G., 1978. *Astrophys. J.*, **220**, 841.
Mitchell, R. M. & Robinson, G., 1981. *Mon. Not. R. astr. Soc.*, **196**, 801.
Mould, J. R. & Hyland, A. R., 1976. *Astrophys. J.*, **208**, 399.
Norman, C. & Silk, J., 1980. *Astrophys. J.*, **238**, 158.
Rydgren, A. E., 1980. *Astr. J.*, **85**, 444.
Schwartz, R. D., 1977. *Astrophys. J. Suppl.*, **35**, 161.
Stapinski, T. E., Rodgers, A. W. & Ellis, M. J., 1979. *Advances in Electronic and Electron Physics*, **52**, 389.
Straede, J. O. & Wallace, P. T., 1976. *Publ. astr. Soc. Pacific*, **88**, 792.
Vrba, F. J., Strom, K. M., Strom, S. E. & Grasdalen, G. L., 1975. *Astrophys. J.*, **197**, 77.